Cell

Cell Flow Reorients the Axis of Planar Polarity in the Wing Epithelium of *Drosophila*

Benoît Aigouy,[1] Reza Farhadifar,[2] Douglas B. Staple,[2] Andreas Sagner,[1] Jens-Christian Röper,[1] Frank Jülicher,[2,*] and Suzanne Eaton[1,*]
[1]Max Planck Institute of Molecular Cell Biology and Genetics, Pfotenhauerstrasse 108, Dresden 01307, Germany
[2]Max Planck Institute for the Physics of Complex Systems, Noethnitzer Strasse 38, Dresden 01187, Germany
*Correspondence: julicher@pks.mpg.de (F.J.), eaton@mpi-cbg.de (S.E.)
DOI 10.1016/j.cell.2010.07.042

SUMMARY

Planar cell polarity (PCP) proteins form polarized cortical domains that govern polarity of external structures such as hairs and cilia in both vertebrate and invertebrate epithelia. The mechanisms that globally orient planar polarity are not understood, and are investigated here in the *Drosophila* wing using a combination of experiment and theory. Planar polarity arises during growth and PCP domains are initially oriented toward the well-characterized organizer regions that control growth and patterning. At pupal stages, the wing hinge contracts, subjecting wing-blade epithelial cells to anisotropic tension in the proximal-distal axis. This results in precise patterns of oriented cell elongation, cell rearrangement and cell division that elongate the blade proximo-distally and realign planar polarity with the proximal-distal axis. Mutation of the atypical Cadherin Dachsous perturbs the global polarity pattern by altering epithelial dynamics. This mechanism utilizes the cellular movements that sculpt tissues to align planar polarity with tissue shape.

INTRODUCTION

The PCP pathway coordinates tissue planar polarity in vertebrate and invertebrate epithelia (Simons and Mlodzik, 2008; Vladar et al., 2009). PCP proteins localize to apical junctions and form intracellularly polarized domains with different compositions. In the *Drosophila* wing, these domains link proximal and distal cell boundaries and orient wing hair outgrowth distally. Distal complexes containing Flamingo (Fmi), a.k.a. Starry night (Stan), Frizzled (Fz), Dishevelled (Dsh) and Diego (Dgo) interact across cell boundaries with proximal complexes containing Fmi, Strabismus (Stbm), a.k.a. Van Gogh (Vang) and Prickle (Pk). In the absence of any single PCP protein, the others do not polarize well and hair outgrowth is misoriented (Seifert and Mlodzik, 2007; Strutt and Strutt, 2005; Uemura and Shimada, 2003). Feedback loops arising from interactions of PCP proteins within and between cells may be sufficient for the local alignment of PCP complexes between small groups of cells (Amonlirdviman et al., 2005; Tree et al., 2002a; Tree et al., 2002b). Proposed cellular mechanisms underlying local feedback loops include preferential interactions between Fmi/Fz and Fmi/Stbm complexes across cell boundaries, and the decreased susceptibility of these complexes to endocytosis (Chen et al., 2008; Strutt and Strutt, 2008; Wu and Mlodzik, 2008). Also, alignment of microtubules may bias the delivery of Fz to the distal side of the cell (Shimada et al., 2006).

While these mechanisms can polarize PCP domains intracellularly and align them locally, less is understood about mechanisms that specify global alignment of PCP domains with the proximal-distal (PD) axis of the wing. The atypical Cadherins Fat (Ft) and Dachsous (Ds), and a regulatory golgi kinase Four-jointed (Fj) influence global orientation of PCP domains by a mechanism that is unclear (Adler et al., 1998; Ma et al., 2003; Matakatsu and Blair, 2004; Strutt and Strutt, 2002; Zeidler et al., 2000). The Fat ligand Ds is expressed highly in proximal regions that give rise to the hinge, but at lower levels in the more distal wing blade, during both larval and pupal stages (Cho and Irvine, 2004; Clark et al., 1995; Ma et al., 2003; Matakatsu and Blair, 2004; Strutt and Strutt, 2002). Fj, which regulates their activity (Ishikawa et al., 2008) is expressed with an opposite pattern (Villano and Katz, 1995; Zeidler et al., 2000). These opposing patterns have been proposed to cause intracellular asymmetries that directly bias accumulation of core PCP proteins in wing cells (Ma et al., 2008, 2003; Strutt and Strutt, 2002; Tree et al., 2002a). However this is not the case in the abdomen where Ft/Ds and PCP proteins act independently to control trichome polarity (Casal et al., 2006). Even in the wing, Ft and Ds do not act at the time that PCP domains actually align with the PD axis, but much earlier (during larval or prepupal stages), to influence the global PCP pattern (Matakatsu and Blair, 2004; Strutt and Strutt, 2002). Ft and Ds regulate both the amount and orientation of proliferation in the larval wing epithelium (Baena-Lopez et al., 2005; Bryant et al., 1988; Clark et al., 1995; Garoia et al., 2005, 2000). It is not yet clear whether this activity is relevant to the PD alignment of PCP proteins during pupal stages.

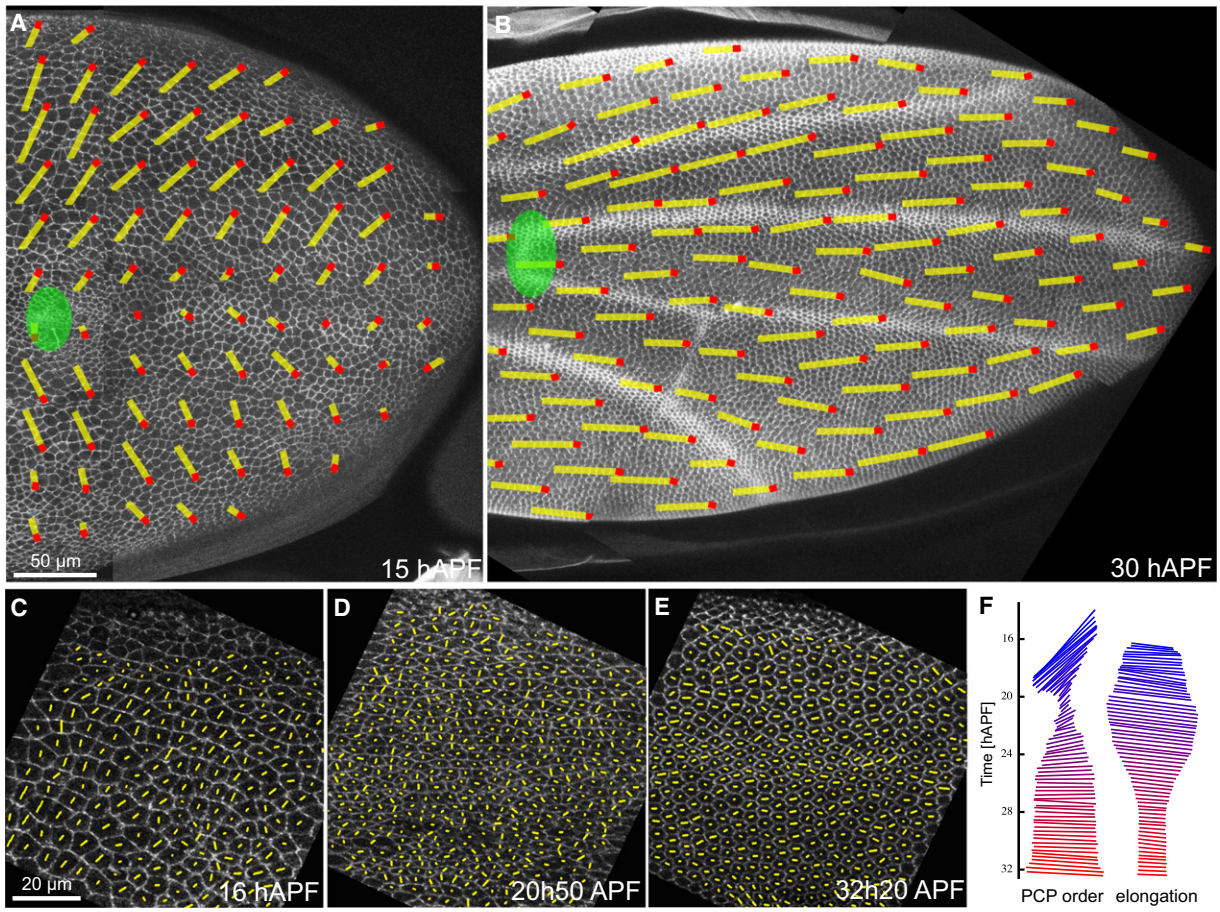

Figure 1. Time Evolution of Planar Polarity

(A and B) The magnitude and axis of average nematic order (yellow bars) overlaid on Stbm:YFP-expressing wings, at 15 hAPF (A) and 30 hAPF (B). Red dots indicate Fz:YFP domain polarity. Green ellipses indicate the anterior crossvein.

(C–E) Stbm:YFP at the indicated times between veins L1 and L3. Yellow bars show the PCP nematic for each cell.

(F) Magnitude (arbitrary units) and axis of average nematic order (left) and cell elongation (right) as a function of time (indicated on the *y* axis and by color) derived from the wing shown in (C–E).

In all figures, anterior is top and proximal is left.

See also Figure S1.

Our previous experiments suggested that PCP domain polarity does not develop de novo during pupal stages; PCP domains are polarized in both larval wing discs and prepupal wings, but polarity is not aligned with the PD axis. At early pupal stages, the PCP axis is oriented at an angle to the PD axis (Classen et al., 2005). Later, by the time wing hairs form, PCP domains are oriented along the PD axis of the wing. Alignment with the PD axis occurs during a phase in which wing epithelial cells are exchanging their cell contacts (Classen et al., 2005). One consequence of remodelling is an increase in hexagonal order of the wing epithelium. Theoretical analysis suggested that different types of fluctuations could guide epithelial cells initially disordered by proliferation toward a hexagonal state (Farhadifar et al., 2007). Here, we investigate the relationship between these cell rearrangements and the temporal evolution of PCP orientation patterns. We quantitatively analyze time-lapses of pupal wing epithelia and combine these data with theoretical analysis to extract key mechanisms that couple cell rearrangements to PCP reorientation.

RESULTS

Planar Polarity Points Initially toward the Wing Margin and Reorients Distally

To investigate how PCP order evolves during pupal development, we imaged wings expressing Stbm:YFP between 15 and 34 hr after puparium formation (hAPF). We developed a method to quantify planar polarity based on the cell perimeter intensity of Stbm:YFP. This method quantifies the axis and magnitude of polarity, but not its vector orientation (Supplemental Theoretical Procedures, 1.1 and Figures S1A–S1E available online). We started by quantifying the axis of PCP at 15 hAPF (Figure 1A); we also determined the polarity vectors in these wings by creating Fz:YFP-expressing clones (Figures S1F–S1H). As

suggested previously (Classen et al., 2005), PCP at early stages is correlated over long distances (Figure S1M) and is oriented such that Fz:YFP domains face the wing margin (Figures 1A and 1C and Figures S1F–S1I). Starting at about 18 hAPF, the magnitude of the average alignment of groups of cells (local nematic order, see Supplemental Theoretical Procedures, 1.2) begins to decrease (Figures 1D and 1F and Figure S1J), and the average axis of alignment begins to rotate toward the PD axis (Figure 1F and Figures S1J and S1K). Reduced alignment reflects both reduced polarity of individual cells and reduced polarity correlation over distance (Figures S1L and S1M). After reaching a minimum about 20 hAPF, the magnitude of average nematic order increases; by 26 hAPF nematic order is again maximal and aligned parallel to the PD axis (Figures 1B, 1E, and 1F, Figures S1J and S1K, and Movie S1). Where we have determined the direction of polarity, we quantify average polar order by a measure ranging from zero to one (one corresponding to perfect alignment) (Supplemental Theoretical Procedures, 1.3). At 15 hAPF, polar order averaged over the whole wing blade is only 0.60, because polarity is oriented differently in anterior and posterior wing regions (Figure 1A). By 32 hAPF average polar order reaches 0.98 (Figure 1B). Thus, PCP domains do not develop polarity de novo during pupal stages, but rather reorient pre-existing polarity.

Polarity reorientation is reflected in the influence of *fz* mutant clones on the polarity of adjacent wild-type tissue. At 15 hAPF, *fz* clones perturb polarity of tissue lying between the clone and the wing margin (Figures S1N and S1O) consistent with the early polarity pattern. After reorientation, polarity is disturbed in wild-type tissue lying distal to the clone (Vinson and Adler, 1987).

We noted that reorientation of PCP correlated with a transient cell shape deformation that elongates cells in the PD axis (Figure 1F). Quantifying elongation (Supplemental Theoretical Procedures, 2) reveals that average polarity shrinks in magnitude and reorients toward the PD axis as cells elongate. The magnitude of average polarity along the PD axis then increases as cell elongation decreases (Figure 1F). The precise temporal correlation of these events suggests that they are controlled by the same underlying mechanisms.

Dramatic Morphogenetic Movements Reshape the Wing during Pupal Development

To explore global changes occurring in the wing as cells change shape and PCP reorients, we imaged ECadherin:GFP-expressing wings at low magnification from 15 to 32 hAPF. Dramatic morphogenetic movements reshape the wing during this time (Figures 2A–2C and Movie S2). At 15–16 hAPF, the hinge and blade regions are roughly equal in size and the shape of the hinge is not yet recognizable (Figure 2A). Between 15 and 24 hAPF, the hinge undergoes patterned contractions that halve its area and shape the allula and costa (Figures 2A–2C, Movie S2, and Movie S3A). While wing-blade area remains constant during this time, wing shape changes – elongating in the PD axis and narrowing in the AP axis (Figures 2A–2C and Movie S2).

To quantify tissue movements underlying this shape change, we tracked different regions and calculated local velocity vectors (Supplemental Theoretical Procedures, 3). As the hinge contracts, wing-blade cells flow proximally toward the hinge at different velocities (Figures 2D–2F, Movie S3B). Between 15 and 18 hAPF, velocities have both inward and proximal components (Figure 2D). Later, flow is proximally oriented and fastest in the middle of the wing blade (Figure 2E). These inhomogeneous velocities define local compression, shear and rotation as cells move with respect to each other (Supplemental Theoretical Procedures, 4). The shear axis in a particular region can be thought of as the local axis of tissue deformation. In the wing, local shear axes are oriented in a fan-like pattern that is roughly symmetric about the third wing vein (Figures 2G–2I, Figures S2J and S2K, and Movie S3C). Although the wing as a whole does not rotate, local rotation does occur and is mainly clockwise anterior to the third wing vein and anti-clockwise posterior to it (Figures 2J–2L, Figure S2L, and Movie S3D). These patterns of shear and rotation lengthen the wing blade in the PD axis and narrow it in the anterior-posterior (AP) axis. Strikingly, the observed antisymmetric rotation pattern would shift early margin-oriented polarity toward the distal direction.

To investigate whether the tissue flows that reshape the wing blade were driven by hinge contraction, we completely severed the hinge from the blade before contraction occurred (Figure 3A). After severing, wing-blade tissue flows distally rather than proximally (Figure 3C and Movie S4A). Shear is reduced and is mainly perpendicular to the PD axis (Figure 3D and Movie S4B), rather than forming a fan-like pattern. Rotation is also reduced, and its orientation is reversed compared to unperturbed wings (compare Figure 3E with Figure 2K, and Movie S4C with Movie S3D). As a result, the wing blade undergoes opposite shape changes to those that normally occur. Nevertheless, wing hairs (not shown) and longitudinal veins (Figure 3B) form normally. These data suggest that hinge contraction exerts mechanical stresses that contribute to the observed cell flow patterns that change the shape of the wing blade.

Cell Boundary Tension Is Elevated along the PD Axis during Hinge Contraction

To ask how cell boundary tension changes during hinge contraction, we used a pulsed UV laser to sever cell boundaries lying at different angles to the PD axis, and monitored the movements of adjacent vertices. The initial velocity with which vertices move apart is a measure of cell boundary tension. Before hinge contraction, tension is similar on all cell boundaries. When the hinge contracts, tension increases specifically on those cell boundaries lying at angles close to that of the PD axis (Figures S3A and S3B). This suggests that hinge contraction exerts forces on the blade that direct cellular flows via an anisotropic stress profile.

Tissue Flow in the Wing Blade Results from Oriented Cell Divisions, Cell Elongation, and Neighbor Exchanges

To investigate the cellular events underlying tissue flow, shear, and rotation, we tracked groups of cells between veins 3 and 4, starting 15 hAPF. This revealed that local tissue shape change occurs in two distinct phases. The first is dominated by oriented cell division and PD cell elongation, and the second by oriented cell rearrangements (Figure 4 and Movie S5A).

During phase I (about 15–24 hAPF), cell elongation increases in the PD axis (Figures 4A–4C and 4G). Cell boundary loss exceeds new boundary formation (Figure 4G), as confirmed by

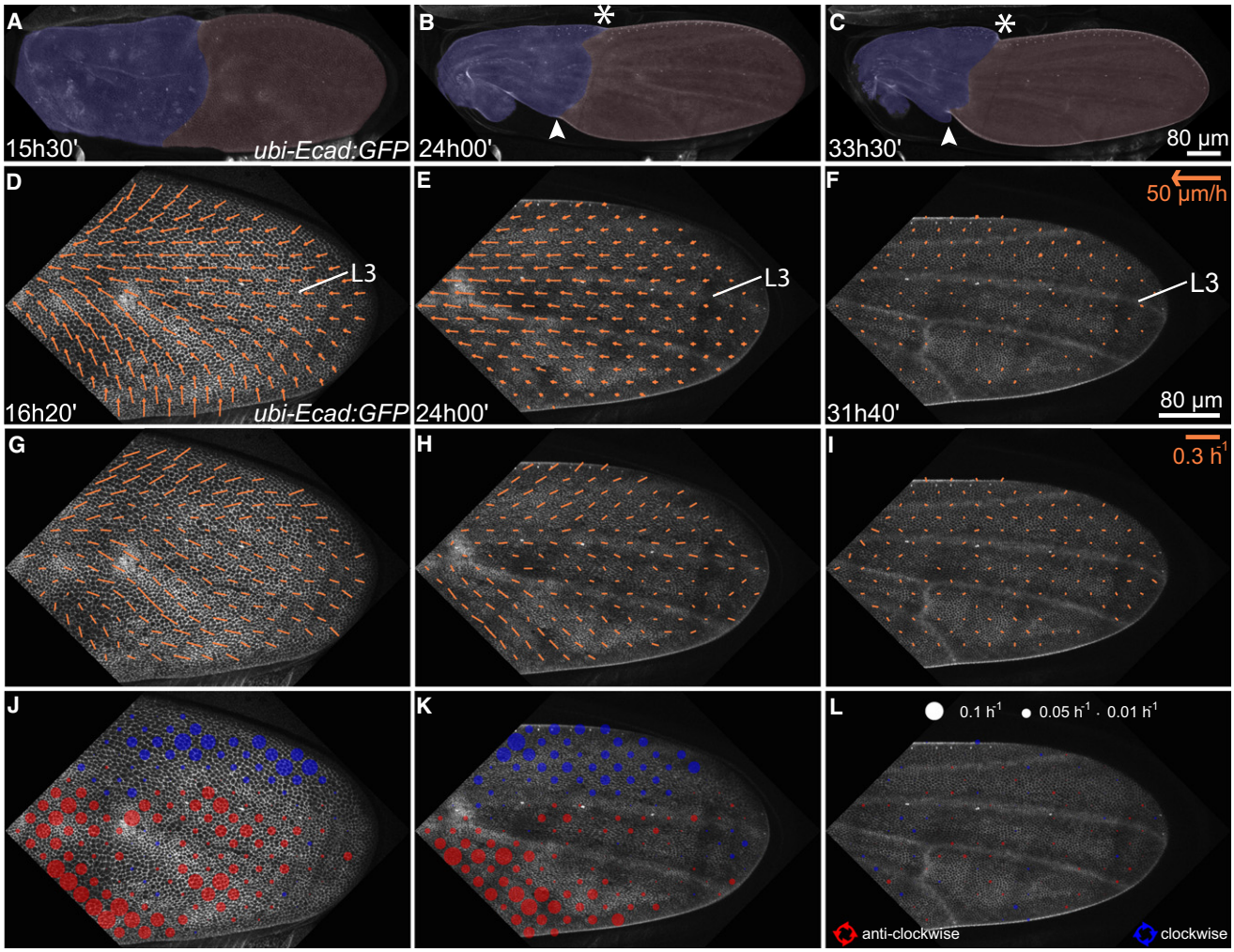

Figure 2. Tissue Shape Changes during Hinge Contraction

(A–C) Wing images from a movie spanning roughly 15-33 hAPF. The hinge (blue) contracts, the wing blade (red) elongates. Allula (arrowhead) and costa (asterisk) are indicated. The area of the wing hinge is 102 × 10^3 μm^2 in (A) and 50 × 10^3 μm^2 in (C). The area of the wing blade is 121 × 10^3 μm^2 in (A) and 127 × 10^3μm^2 in (C).

(D–L) Locally averaged features of the cellular flow field at indicated times.

(D–F) Flow velocity vectors. Speed corresponds to arrow length as indicated.

(G–I) Rate and axis of pure shear. Bar length indicates shear rate.

(J–L) Local rotation rate (indicated by circle size) in radians per hour.

L3 indicates the third longitudinal vein.

Results shown are representative of five separate experiments.

See also Figure S2.

the decrease in average neighbor number (Figure 4F). These new cell boundaries have no preferred direction during phase I (Figure 4I). Cells undergo between one and two rounds of oriented cell division that reduce cell size. Between veins 3 and 4, these divisions are on average oriented 20° to the PD axis (Figure 4H). As phase I ends, cell elongation peaks (Figure 4G) and cell division stops (Figure 4F). At the end of this phase, tracked tissue patches have deformed in a way that can be accounted for by the combination of cell elongation and oriented cell division. During phase II (about 24–32 hAPF), cells assemble new contacts parallel to the PD axis (Figures 4G and 4I). These oriented neighbor exchanges relieve cell elongation (Figure 4G) and stabilize the tissue shape change caused by cell elongation during phase I (Figures 4C–4E). They also increase average neighbor number and the fraction of hexagonally packed cells (Figure 4F).

Severing the Hinge from the Wing Blade Blocks PD Elongation and Misorients Cell Divisions and Neighbor Exchanges

To investigate the cellular basis of altered shear and rotation in severed wing blades, we quantified cell elongation and the orientation of neighbor exchanges and cell divisions after severing from the hinge (Figures S3C–S3G and Movie S5B).

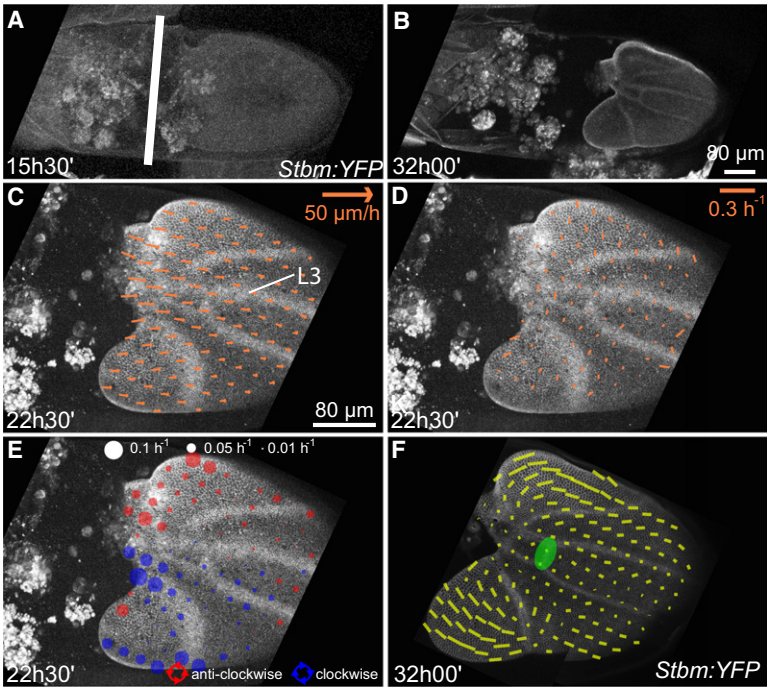

Figure 3. Tissue Shape Changes in Severed Wings

(A and B) Images taken at the indicated times from a movie spanning 15–32 hAPF. The hinge was severed from the blade along the line indicated.

(C–E) Locally averaged features of the cellular flow field at 22h30′ APF.

(C) Flow velocity vectors. Speed corresponds to arrow length as indicated.

(D) Rate and axis of pure shear. Shear rate corresponds to bar length as indicated.

(E) Local rotation rate (indicated by circle size) in radians per hour.

(F) Magnitude and axis of average nematic order (yellow bars) overlaid on a severed Stbm:YFP-expressing wing at 32 hAPF. Green ellipse = anterior crossvein. L3, third longitudinal vein. Results shown are representative of four separate experiments.

Cell divisions are strongly oriented in unperturbed wings. When the hinge is severed from the blade, cell division continues (Figure S3H), but the angle of cell division is more disperse (Figure S3J). In addition, these cells do not elongate further along the PD axis (Figure S3I), becoming instead more isotropic. While neighbor exchanges still occur, their axis is shifted with respect to unwounded wings, lying at ±45 degrees with respect to the PD axis (compare Figure S3K to Figure 4I). Finally, wing severing reduces the final number of hexagonally packed cells (62.44% ± 3.5% in wounded wings [n = 3] versus 77% ± 4.8% in unperturbed wings [n = 5]). Thus, severing the wing dramatically changes the observed patterns of cell elongation, cell division, and rearrangements. This suggests that anisotropic stress caused by hinge contraction has a key role in guiding the tissue flow that reshapes the wing blade. It also suggests that cell flow increases hexagonal packing, similar to the annealing effect of cell boundary fluctuations (Farhadifar et al., 2007).

Severing the Hinge Alters the Global Pattern of Planar Polarity

Reorientation of planar polarity in the intact wing occurs at the same time that the wing blade is reshaped by hinge contraction, suggesting that these events depend on one another. The observed pattern of clockwise and anti-clockwise tissue rotation tends to reorient early margin-directed polarity toward the PD axis. In addition, the shear pattern presages the final orientation of planar polarity (Figure 2H). To ask whether tissue movements induced by hinge contraction guided polarity reorientation, we examined the distribution of Stbm:YFP in wing blades that had been severed from the hinge before contraction. In severed wings, the global PCP pattern differs from that of the intact wing (compare Figure 1B with Figure 3F), suggesting that polarity is altered by the changed patterns of cell rearrangements, cell division, and cell elongation. This implies that cell flows guide reorientation of PCP.

Oriented Cell Boundary Assembly Increases the Visibility of Planar Polarity

While the majority of polarity reorientation occurs during phase I, average PCP order increases in magnitude during phase II, as cells extend new contacts mostly parallel to the PD axis and develop hexagonal packing geometry (Figure 1F and Figures 4F and 4I). Could the increase in polar order be related to these processes? To investigate this, we imaged PCP protein localization as new cell boundaries formed (Figures 5A–5F and Movie S5C). We noted that Stbm:YFP had a clustered rather than a uniform distribution on cell boundaries throughout pupal development. Even at early stages, these clusters contain both Stbm:YFP and Fz:CFP, suggesting that they constitute PCP protein complexes (Figures S4A–S4C). Consistent with this, Stbm:YFP clustering is reduced in *fz* mutant tissue (Figures S4D and S4E). Individual clusters are persistent and can be tracked for several hours. However, proteins within them turn over more rapidly (Figures S4G–S4I). Clusters do not form rapidly on new cell boundaries derived either from cell division or neighbor exchange (Figure 5 and Movie S5C). During phase II, new cell boundaries, expanding parallel to the PD axis within minutes, typically remain devoid of these clusters for hours (Figures 5A–5H). Consequently, Stbm:YFP clusters become restricted mainly to older cell interfaces on the proximal and distal sides of the cell. Thus, oriented cell boundary expansion and the concomitant increase in hexagonal packing order ensure that PCP clusters become well separated within cells and better aligned between cells; even though PCP has already reoriented during phase I, oriented cell boundary expansion during phase II tends to increase the average nematic order (compare Figure S4F with Figures S1A—S1E).

A Theoretical Analysis of Polarity Reorientation

While local tissue rotation clearly implies local rotation of the polarity axis, it is less simple to understand how tissue shear affects the axis of planar polarity. Tissue shear is caused by

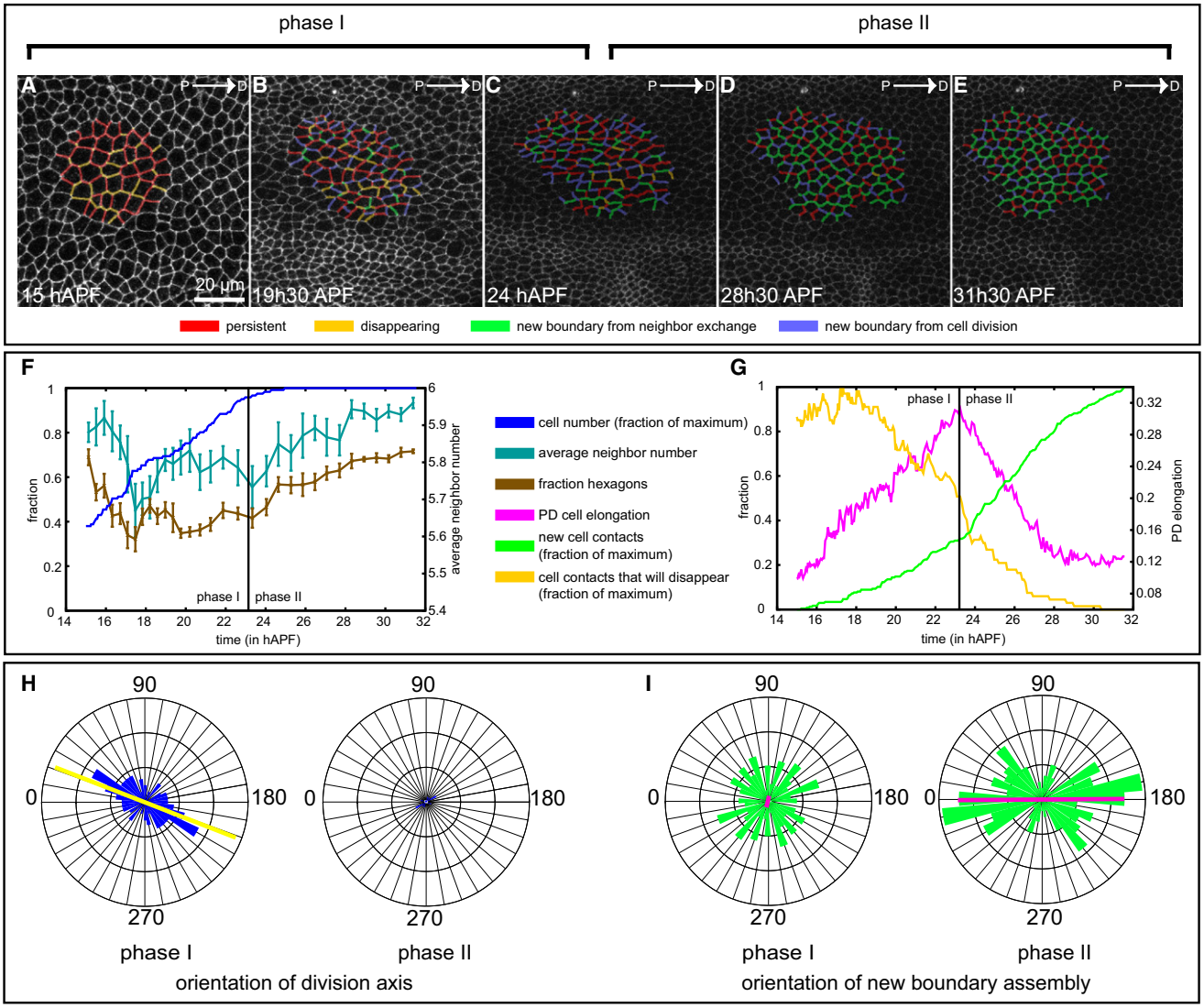

Figure 4. Cell Elongation, Division, and Rearrangement

(A–E) A group of cells anterior to the posterior crossvein was tracked between 15h and 31h30′ APF. Cell boundaries are color-coded depending on their fate: red boundaries persist indefinitely, yellow boundaries disappear, green boundaries form during the movie as a result of neighbor exchange, and blue boundaries form between daughter cells upon division.

(F and G) Quantification of cellular changes in the patch of tissue tracked in (A–E). Fraction of maximal cell number (dark blue), average neighbor number (light blue, averaged over five frames), fraction of hexagonal cells (brown, averaged over five frames), PD cell elongation (magenta, average maximum value = 0.388 ± 0.053, n = 5), fraction of boundaries that will disappear (yellow), and the fraction of newly formed boundaries from neighbor exchange (green).

(H and I) Angular distribution of cell divisions (blue) (H) and new cell boundaries (green) (I) at the end of phase I and phase II. Yellow and magenta bars indicate average angle of nematic order of cell division (yellow) and new cell boundary formation (magenta) (see Supplemental Theoretical Procedures). Bar length indicates the degree of focus (magnitude of average nematic order, ranging from 0 to 1, see Supplemental Theoretical Procedures, 1.2). The outer circles in (H) and (I) correspond to magnitude = 0.4. Average magnitude of phase I cell division order is 0.44+/−0.12, n = 4. Average magnitude of new boundary formation order in phase II = 0.35+/−0.04, n = 4.

Data are presented as mean ± SD.

See also Figure S3.

oriented cell divisions, cell elongation, and oriented cell rearrangements. Because microtubules have been shown to align with the axis of cell elongation (Cortes et al., 2006; Daga and Nurse, 2008; Haase and Lew, 2007; Strauss et al., 2006), cell shape may directly influence the distribution of PCP within the cell. Indeed, microtubules in wing epithelial cells align with the PD axis at this time (Shimada et al., 2006). We turned to theoretical analysis to explore how each of these processes might affect the axis of planar polarity. Previously, we used a vertex model to study the effects of proliferation on cell packing geometry (Farhadifar et al., 2007). Here, we add to this model a simplified description of the dynamics of PCP order.

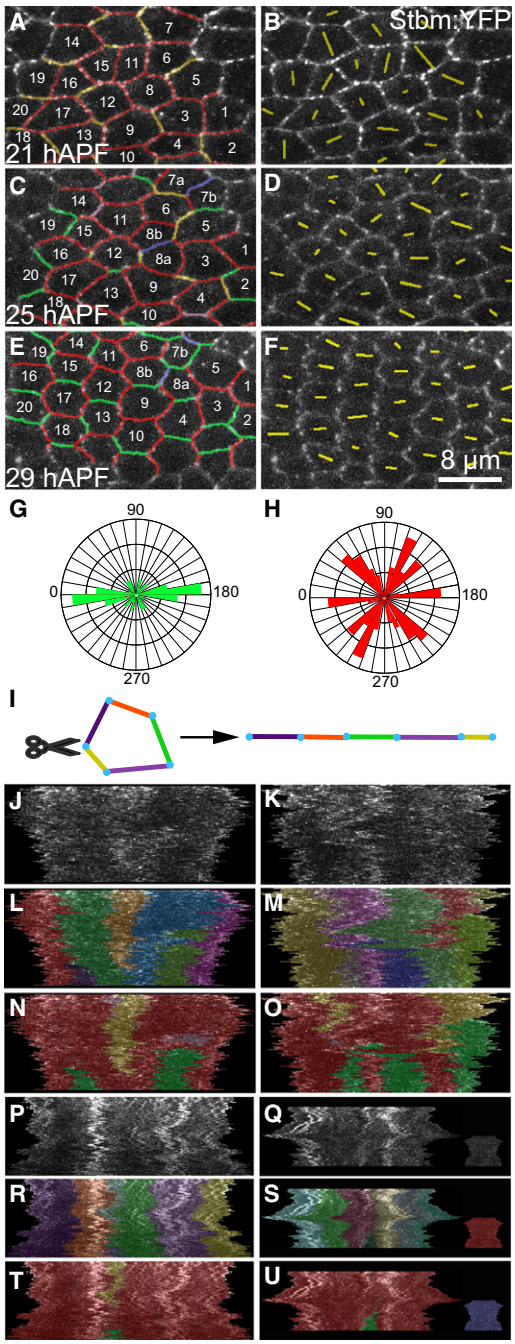

Figure 5. Cell Rearrangements Increase the Visibility of PCP

(A–F) Images from a 21–29 hAPF movie of a Stbm:YFP-expressing wing. In (A), (C), and (E), cell identity is indicated by numbers and cell boundaries are colored according to their fate as in Figure 4. (B), (D), and (F) show PCP nematics for each cell (yellow).

(G and H) Angular distribution of newly formed (green, [G]) and permanent boundaries (red, [H]).

(I) Each kymograph line depicts the linearized perimeter of a selected cell at time t.

(J–O) Perimeter intensity kymographs for two cells of the movie (frame rate = 6′, movie length = 8 hr) shown in (A–F). In (L) and (M), each boundary is identified by a random color. Colors in (N) and (O) indicate boundary fate (see Figure 4). Permanent boundaries (red in [N] and [O]) carry PCP clusters that persist for 8 hr. New boundaries (green in [N] and [O]) remain devoid of Stbm:YFP clusters.

(P-U) Kymographs of a nondividing cell (P), (R), and (T) or a dividing cell (Q), (S), and (U) between 20-21 hAPF (30′ frame rate). In (R) and (S), each boundary is identified by a random color. Colors in (T) and (U) indicate boundary fate (see Figure 4). After cell division (Q), (S), and (U) depicts the joint perimeter of the two daughter cells and the boundary created by cell division (blue in [U]) separately.

See also Figure S4.

A Physical Description of PCP in the Vertex Model

Cell shape, as defined by the network of adherens junctions, can be described as force-balanced configurations in a vertex model, in which an arrangement of cells is represented by a set of cell bonds. This model takes into account cell mechanics, cell adhesion and cell division (Farhadifar et al., 2007). Our description of PCP order is based on attractive interactions between proximal and distal PCP domains across cell boundaries and repulsive interactions within cells. This differs from previous approaches (Amonlirdviman et al., 2005; Le Garrec et al., 2006), in that we do not attempt to describe all details of interactions between PCP proteins, but rather consider effective interactions between proximal and distal domains. Each cell bond i, separating cells α and β, is assigned two variables, σ_i^α and σ_i^β, which describe the level of PCP proteins on either side of this bond (Figure 6A). The variables σ_i^α can take continuously varying values; $\sigma_i^\alpha = 1$ corresponds to a high level of proximal proteins (blue), while $\sigma_i^\alpha = -1$ corresponds to a high level of distal proteins (red). We introduce a potential function for interactions of PCP domains:

$$E = J_1 \sum_i \sigma_i^\alpha \sigma_i^\beta - J_2 \sum_{\{i,j\}} \sigma_i^\alpha \sigma_j^\alpha - J_3 \sum_\alpha \varepsilon^\alpha \cdot \boldsymbol{Q}^\alpha, \qquad (1)$$

where J_1 and J_2 are PCP interaction parameters and J_3 describes coupling of PCP to cell elongation (for $J_3 = 0$, PCP does not couple to cell elongation). For $J_1 > 0$ the potential favors interactions between proximal and distal proteins across cell bonds. For $J_2 > 0$, accumulation of proximal and distal proteins on neighboring bonds within a given cell is disfavored. For $J_3 > 0$, alignment of PCP with the long axis of the cell is favored: this is motivated by the idea that aligned microtubules bias the transport of PCP proteins (Shimada et al., 2006). The first sum is over all bonds i, the second sum is over all pairs $\{i,j\}$ of adjacent bonds in the network, and the third sum is over all cells α. The cell shape and PCP nematic order are described by the tensors ε^α and $\boldsymbol{Q}^\alpha$, respectively (Supplemental Theoretical Procedures, 5). We introduce a time evolution of PCP level on cell bonds: $d\sigma_i^\alpha/dt = -\gamma \partial E/\partial \sigma_i^\alpha$, where t is time and γ is a kinetic coefficient that determines the PCP relaxation time $\tau = 1/(\gamma J_1)$. We solve these dynamic equations numerically, imposing two constraints: (1) in each cell, amounts of proximal and distal proteins are equal and (2) these amounts do not change with time (Supplemental Theoretical Procedures, 5).

Global Polar Order Generated by Network Growth

To examine how different types of shear reorient polarity, we must start from a cellular configuration in the vertex model with

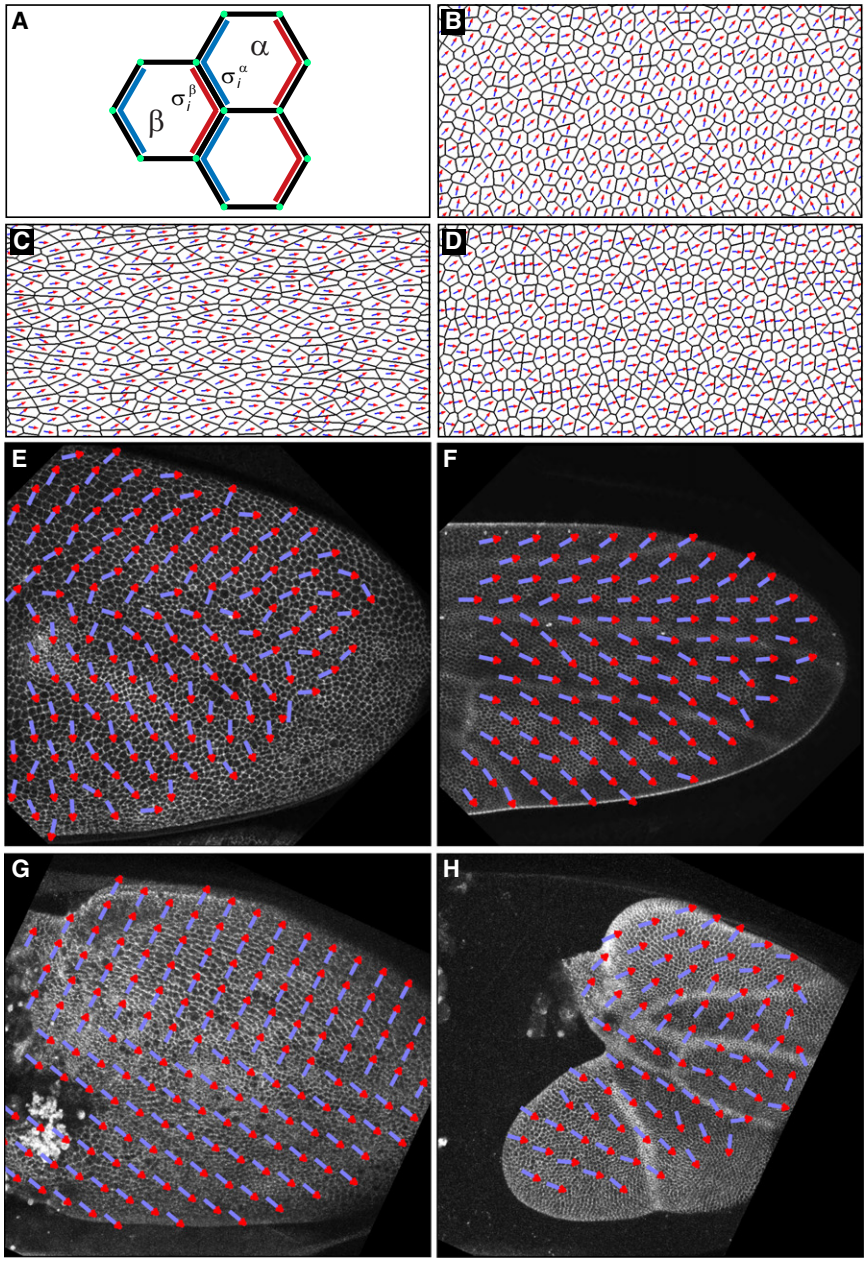

Figure 6. Theoretical Analysis of Shear and Rotation on the Reorientation of Planar Polarity

(A) Schematic representation of PCP in the vertex model. The variables, σ_i^α and σ_i^β, represent the level and type of PCP domains on bond *i* shared by cells α and β.

(B) Cell packing with PCP order generated by simulated proliferation in the vertex model with PCP dynamics, starting from 36 randomly polarized cells with $k_d\tau$ = 0.01, J_2/J_1 = 0.5 and J_3 = 0. Arrows in (B)–(D) show the direction of polarity.

(C and D) Reorientation of polar order by shear due to external forces (C) or oriented cell division (D). Starting from the network (B), and simulating shear along the horizontal axis, leads to the networks shown. Parameter values for (C) are $k_d\tau$ = 0.01 and J_3/J_1 = 0.05. For (D), $k_d\tau$ = 0.01, J_3 = 0 and ~3 rounds of cell division were simulated. The shear generated corresponds to an aspect ratio of 4 in (C) and 1.5 in (D).

(E and F) Calculations of polarity reorientation based on Equation 2 and measured patterns of shear and rotation. Starting with the observed early polarity (E), the time evolution described by Equation 2 with $\nu = -3$ generates a final PD pattern (F). The wing is the same as that shown in Figures 2D–2L.

(G and H) same procedure as in (E and F) applied to the wounded wing shown in Figure 3 with $\nu = 2$. We start with an initial pattern mimicking the early polarity (G).

See also Figure S5.

globally aligned PCP variables. To generate such a configuration without an external bias is nontrivial (Burak and Shraiman, 2009). Surprisingly, a simple and general way to generate large networks with long-range polarity is to start from a small group of cells with an initially random PCP configuration (random values of σ_i^α, Supplemental Theoretical Procedures, 6). This network is then expanded by simulating stochastic cell divisions at a rate k_d. Simultaneously, the dynamic equations for the PCP variables are solved. Interactions of PCP variables generate local order, which aligns over the whole network when it is still small. Order is maintained during growth and leads to globally aligned polarity in the resulting large networks if the PCP relaxation time τ is sufficiently fast ($k_d\tau$<1, Figures 6B, Figure S5A, and Movie S6A). This is consistent with the observation of global PCP patterns in the growing wing disc (Classen et al., 2005), and suggests that these patterns arise early during development.

Shear Reorients the Polarity Axis in the Vertex Model

Starting with a globally polarized network, we used the vertex model to examine how different types of shear could influence the average polarity orientation of groups of cells. We first studied the effects of shear caused by cell elongation and oriented cell rearrangements. In our simulations, we induced pure shear at a rate k_s by forcing the network to elongate along one axis at constant total area (Supplemental Theoretical Procedures, 6). We oriented the initial axis of average polarity at an angle of 45 degrees to this shear axis (Figure 6B). As the network is deformed, cells elongate and undergo T1 transitions that are oriented along the stretch axis. We find that shear reorients polarity either parallel or perpendicular to the shear axis, depending on the value of $k_s\tau$ and on the strength J_3 of the coupling of cell shape to PCP distribution (Figures 6C, Figures S5B–S5D, and Movies S6B—S6C). Reorientation occurs during

a characteristic time $1/|2\nu k_s|$, where ν is a dimensionless coefficient. We define ν to be negative if polarity aligns with the shear axis, and positive if it aligns perpendicular to this axis. Positive values of J_3 promote the alignment of the polarity vector with the shear axis, as do faster relaxation times τ of PCP (Figures S5B–S5D). Network configurations generated by this process are irregular and cells are stretched. We relaxed these networks by introducing fluctuations of cell bond tension (Supplemental Theoretical Procedures, 6). This reduced cell stretch and increased both the fraction of hexagons and the magnitude of average polar order, similar to what is observed during phase II in vivo (Figures 4F and 4G, and Figure S5E).

We next studied whether shear generated by oriented cell divisions reorients polarity. We imposed cell divisions in the vertex model at rate k_d oriented at an angle of about 45 degrees to the initial polarity axis (Supplemental Theoretical Procedures, 6). Oriented cell division generates shear parallel to the cell division axis (defined as the line connecting the centers of the two daughter cells) at a rate $k_s = \mu k_d$, where μ depends on network mechanics. We find again that polarity is reoriented either parallel or perpendicular to the shear axis and that the dynamics of reorientation can be characterized by the coefficient ν defined above (Figure 6D, Figure S5F, and Movie S6D). Again, faster relaxation times τ of PCP promote alignment of the polarity vector with the shear axis (Figure S5F).

An Effective Description of Large-Scale Polarity Reorientation by Flow

The reorientation of average polarity by shear flow that we observe in the vertex model is well known in complex fluids such as liquid crystals. In these systems, polarity reorientation is determined by local rotation and shear rates of the flow field and can be described by the following equation (de Gennes and Prost, 1993; Joanny et al., 2007)

$$\frac{\partial\theta}{\partial t} = \nu k_s \sin 2\theta + \omega. \quad (2)$$

Here, ω is the local rotation rate, and k_s is the rate of pure shear (Supplemental Theoretical Procedures, 7). The orientation of polarity is described by the angle θ, relative to the axis of pure shear. The coefficient ν describes how pure shear influences reorientation of polarity. In the absence of rotation, $\omega = 0$, pure shear aligns polarity either with the shear axis $(\theta = 0)$ or perpendicular to it $(\theta = \pi/2)$ depending on the sign of ν. In liquid crystals, the value of ν depends on molecular geometries and intermolecular interactions (de Gennes and Prost, 1993). In the absence of pure shear, $k_s = 0$, local tissue rotations reorient polarity as $\partial\theta/\partial t = \omega$.

Equation 2 for $\omega = 0$ describes the main features of polarity reorientation by pure shear in the vertex model described above. The coefficient ν that characterizes how shear affects reorientation in the vertex model is the same as the parameter ν in Equation 2. We can thus use Equation 2 to determine quantitatively how the observed patterns of rotation and shear reorient the global pattern of planar polarity in the wing.

Starting with the observed polarity pattern at 15 hAPF, we locally applied Equation 2, with ν being the only free parameter, to calculate the corresponding time-dependent reorientation of polar order. Local rates of rotation and shear were obtained from the experimentally determined flow field between 15 and 32 hAPF. To ask to what extent local rotation alone could reproduce the observed polarity reorientation, we first considered $\nu = 0$, i.e., shear does not influence reorientation. In this case polarity realigns toward the PD axis, however, the final average polar order achieved is only 0.76 (77% of the experimental value at 32 hAPF). Thus, local rotation can account for only part of the observed reorientation of the polarity axis.

If ν is nonzero, shear also influences reorientation. Repeating this calculation for different values of ν shows that the final average polar order is largest for $\nu \approx -3$, reaching a value of 0.90 (92% of the experimental value, Figures S5G–S5J). For ν within the range $-10 < \nu < -1$ the polarity field reorients robustly to reach an average polar order of at least 0.85 (Figure S5K, 6E,F and Movie S6E), tolerating small deviations from the experimentally determined pattern of initial conditions (Figure S5K). Note that the effects of local shear on polarity orientation depend on PCP domain interactions and dynamics, as captured in the vertex model. In the calculations using Equation 2, these effects are represented via the value of the parameter ν. However, in writing Equation 2 we choose to neglect interactions of average polar order between neighboring patches of tissue to highlight the role of shear and rotation. We expect such additional interactions could account for the remaining deviation between the solution to Equation 2 and the observed final polarity. Note also that positive values of ν produce a final polarity pattern with lower polar order than rotation alone ($\nu = 0$) (Figure S5K). This analysis suggests that shear caused by the combination of oriented cell divisions, cell elongation and cell rearrangement plays an important role in aligning polarity parallel to the shear axis by a process that is characterized by a negative value of ν. The close agreement between the polarity pattern generated by Equation 2 (Figure 6F) and experimental observations (Figure 1B) provides strong evidence that tissue remodelling is responsible for reorienting the axis of planar polarity.

To ask whether Equation 2 could describe the polarity defects observed when the hinge and wing blade are severed, we used it to calculate polarity reorientation given the shear and rotation patterns measured for these wings. For wounded wings, we find that Equation 2 describes the main features of polarity reorientation provided that ν is positive (Figures 6G and 6H, Figures S5L and S5N, and Movie S6F). This implies that, in wounded wings, shear tends to align polarity perpendicular to the shear axis, rather than parallel to it, as it does in unperturbed wings. Why should shear affect polarity differently in wounded wings? In simulations of the vertex model, we observed that shear generated by oriented cell divisions and by external stresses reorients polarity with different characteristics (Figures S5B–S5D and S5F). The value of ν thus depends on the types of cell shape changes and rearrangements occurring during shear. In wounded wings, where mechanical boundary conditions are perturbed, the remodeling processes that dominate shear differ from those in unperturbed wings (compare Figures S3C–S3K with Figure 4).

In early pupal wings, *fz* clones nonautonomously reorient polarity of adjacent wild-type tissue lying between the clone and the wing margin (Figure S1N and S1O). But after remodeling,

the location of affected wild-type tissue is distal to the *fz* clone (Vinson and Adler, 1987). We wondered whether the shear and rotation observed during remodeling could account for repositioning of affected wild-type tissue. To investigate this, we first simulated growth in the vertex model mimicking the situation of a *fz* mutant clone. Starting with a network of 36 cells, we chose a single cell and set $\sigma_i^\alpha = 1$ on all its bonds (corresponding to loss of Fz domains). We then simulated growth of the network while simultaneously solving the dynamic equation of the PCP network (Supplemental Theoretical Procedures, 5), keeping $\sigma_i^\alpha = 1$ in the simulated clone (indicated in blue). In these simulations, the polarity pattern becomes distorted on one side of the clone as domains with $\sigma_i^\alpha < 0$ (red) are positioned to face the clone (compare Figure S5O with S5Q). These simulations generate PCP patterns that mimic domineering nonautonomy observed in vivo for *fz* and *stbm* mutant clones. Such patterns suggest the interesting possibility that domineering nonautonomy may arise during growth of the wing and may explain why the polarity of wild-type tissue is already reoriented by *fz* clones at 15 hAPF. We use these patterns as initial conditions to study reorientation during shear.

To investigate the effects of shear and rotation on the perturbed PCP polarity patterns, we solve Equation 2 with $\nu = -3$ for both networks with and without simulated clones, and an initial average polarity axis lying 45° to the horizontal (mimicking margin-oriented polarity). We impose shear and rotation at constant rate, with the shear axis oriented horizontally (corresponding to the PD axis of the wing) (Supplemental Theoretical Procedures, 8). This reorients the global polarity of both networks and shifts the perturbed region toward the "distal" side of the clone (compare Figure S5P and R) consistent with experiments (Vinson and Adler, 1987).

Ds Guides Global Planar Cell Polarity by Influencing Epithelial Dynamics

Perturbing the Ft/Ds pathway misaligns PCP domains, but the underlying mechanism is controversial (Axelrod, 2009; Casal et al., 2006; Lawrence et al., 2007; Ma et al., 2003; Tree et al., 2002a). These mutations also cause shorter, broader wings – at least in part by perturbing oriented cell divisions in larval discs (Baena-Lopez et al., 2005). To investigate whether Ds also influenced pupal epithelial remodelling, we analyzed time-lapses of *ds* pupal wings expressing ECadherin:GFP. At 15 hAPF, *ds* wings are already misproportioned; the hinge is overgrown and the wing blade is short and broad (Figure 7A), consistent with altered larval growth. Nevertheless, the hinge contracts as it does in wild-type, reducing its area about twofold (Figures 7A and 7B). Thus, Ds is not required for hinge contraction. Calculating shear and rotation over the whole blade is difficult in *ds* mutants because the epithelium folds; in regions that can be quantified, rotation rates are smaller than in wild-type (Figures S2G–S2I′ and S2L and Movie S7A). However, differences in the shear patterns could not be resolved (Figures S2D–S2F′).

A clearer picture emerged from analyzing *ds* mutants at the cellular level (Figures 7D–7H and Movie S5D). PD cell elongation is reduced in *ds* wings (compare Figure 4G and Figure 7J), and the axis of cell division is less focused than in wild-type (compare Figures 4H and 7K). Thus Ds is required to tightly focus cell division orientation in both larval and pupal wings. Simulations suggest that both cell elongation and oriented cell divisions can reorient polarity (Figures 6C and 6D). Interestingly, both are perturbed in *ds* mutants.

Ds influences both larval and pupal epithelial dynamics—so which is most important for development of PD polarity? To investigate this, we altered Ds levels in the posterior compartment of the wing either throughout development or only during larval growth or after pupariation. Overexpressing Ds throughout wing development causes strong polarity defects in both posterior and anterior compartments (Figure S6A). Overexpressing Ds during larval or pupal development alone causes much milder polarity defects (Figures S6A–S6C). We obtain complementary results by lowering Ds levels. Inducing RNAi against Ds in the posterior compartment throughout development perturbs polarity strongly in both anterior and posterior compartments (Figure S6D). Ds knock-down during larval or pupal development alone causes milder polarity defects (Figures S6E and S6F). These data suggest that Ds is needed both during growth and subsequent epithelial remodelling to ensure proper alignment of PCP with the PD axis. Ds loss or overexpression throughout development causes cumulative defects stronger than those caused by stage-specific perturbation.

Loss of Ds during pupal stages may perturb PD polarity by reducing cell elongation or misorienting cell divisions during remodelling. How could loss of Ds during larval growth affect evolution of PD polarity? One possibility is that Ds-dependent oriented cell divisions in the wing disc guide development of early margin-oriented polarity; complex global PCP patterns are as already seen in the third instar, and prepupal wings show a pattern consistent with margin-oriented polarity (Classen et al., 2005). To test this, we quantified the Stbm:YFP pattern in *ds* wings at 15 hAPF. The pattern of average nematic order in *ds* wings deviates from that of wild-type over large regions, although PCP domains are well aligned locally, (compare Figure 7C and Figure 1A). These observations together with simulations suggest that the larval pattern of oriented cell divisions contributes to development of margin directed polarity. Loss of Ds may perturb the early polarity pattern indirectly by misaligning larval cell divisions.

To ask whether abnormal early polarity in combination with the altered flow pattern could in principle produce normal PD polarity, we started with the altered polarity observed in early *ds* wings and applied the mutant velocity field using Equation 2. For all values of ν, polarity fails to orient as it does in wild-type (average polar order < 0.67, compare Figure S5M with S5K). Taken together, these studies indicate that development of PD polarity depends both on correct initial polarity and on tissue rotation and shear produced during hinge contraction.

Although Ds is expressed at high levels in the hinge and at low levels in the wing blade, this discontinuity along the PD axis is not required to direct PD orientation of PCP domains. Uniform Ds expression rescues polarity in a *ds* mutant background (Matakatsu and Blair, 2004 and Figure S6G-I). Furthermore, lowering Ds levels in the wing blade perturbs polarity more than knock-down in the hinge (Figure S6K,L). In contrast, discontinuities in Ds levels along the AP axis do perturb polarity at a distance; overexpression or loss of Ds in the posterior compartment

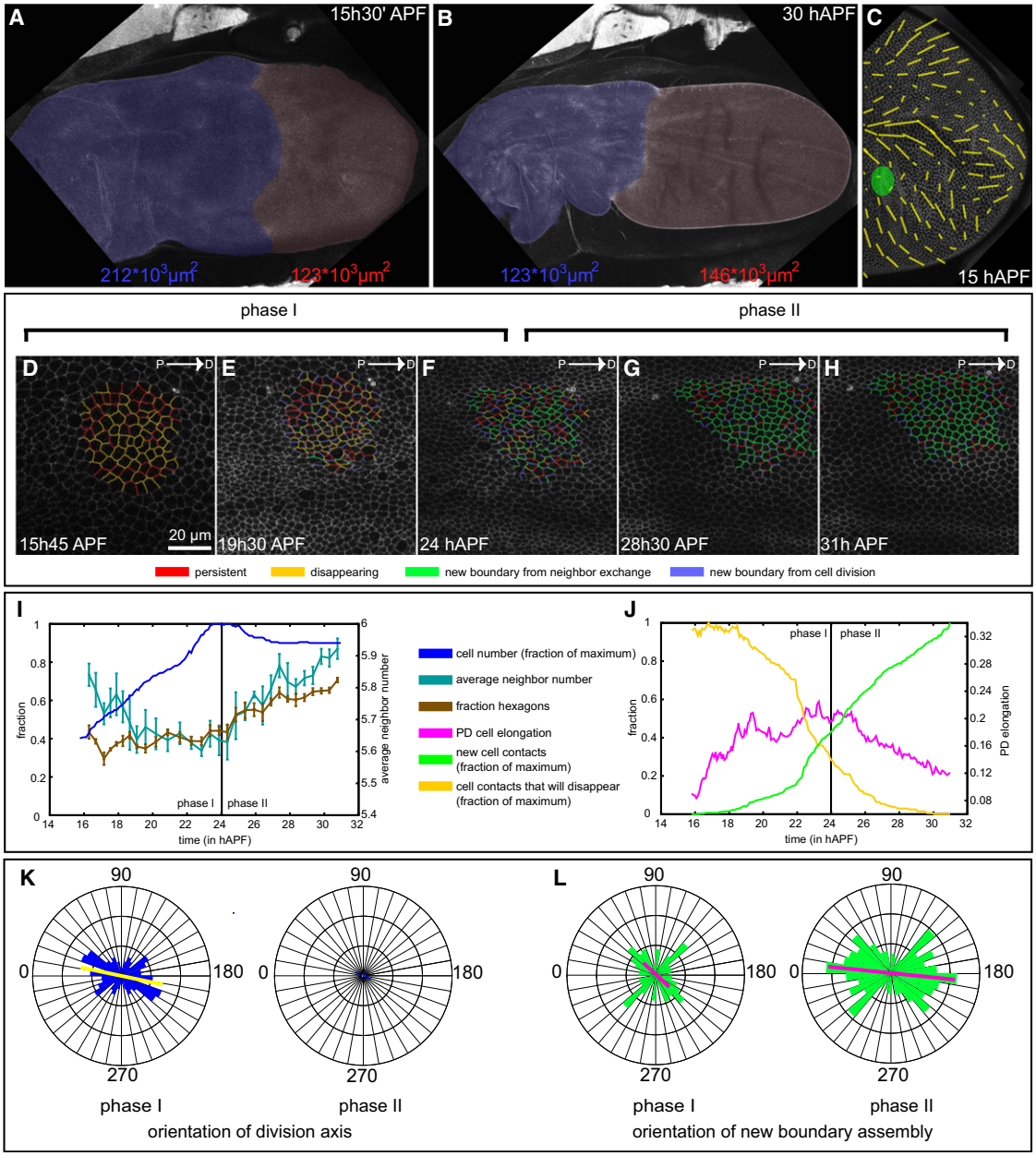

Figure 7. Early Polarity, Cell Elongation, Division, and Rearrangement Are Perturbed in *ds*^{05142} Wings

(A and B) A *ds*^{05142}, *ubi-ECad:GFP* wing at 15h30′ and 30 hAPF. The hinge is colored blue and the blade red. Numbers indicate blade and hinge areas in µm^2.

(C) Average nematic order in a *ds*^{05142},*act-stbm:YFP*/ *ds*^{05142} wing at 15 hAPF (compare to Figure 1A).

(D–H) A group of cells anterior to the posterior crossvein in a *ds*^{05142}, *ubi-ECad:GFP* wing was tracked between 15h45′ and 31 hAPF. Cell boundaries are color-coded as in Figure 4A.

(I and J) Quantification of cellular changes in the patch of tissue tracked in (D–H). Fraction of maximal cell number (dark blue), average neighbor number (light blue, averaged over 8 frames), fraction of hexagonal cells (brown, averaged over 8 frames), PD cell elongation (magenta, average maximum values = 0.243, n = 2 (0.2245, 0.261), fraction of boundaries that will disappear (yellow), and fraction of new boundaries resulting from neighbor exchange (green).

(K and L) Angular distribution of cell divisions (blue) (K) and new boundaries (green) (L) at the end of Phase I and Phase II. Yellow and magenta bars indicate average angle of nematic order of cell division (yellow) and new cell boundaries (magenta) (see Supplemental Theoretical Procedures and Figure 4). Average magnitude of phase I cell division order is 0.145 (0.180, 0.109 n = 2). Average magnitude of new boundary formation order in phase II = 0.338 (0.278, 0.398; n = 2).

See also Figure S6.

nonautonomously perturbs polarity anteriorly (Figures S6A–S6F). Altering Ds levels changes the response of wing epithelial cells to hinge-dependent pulling forces (Figure 7). We therefore considered the possibility that local changes in cell rearrangement and elongation could alter large-scale cellular flows and thus the patterns of shear and rotation in wild-type regions. Indeed, Ds overexpression in the posterior compartment nonautonomously reverses local tissue rotation in anterior cells near the compartment boundary (compare Figures S6M–S6O, Figures 2J–2L, and Movie S7B). These observations suggest that, to generate normal flow patterns in response to hinge contraction, cells in the anterior and posterior compartments must react similarly to mechanical stress.

DISCUSSION

The mechanisms that couple tissue shape to the planar polarity of constituent cells are not well understood. Here, we describe a novel morphogenetic event that both shapes the wing of *Drosophila,* and orients global planar polarity of wing cells. We show that the hinge region contracts shortly after the prepupal to pupal transition. This contraction not only shapes the wing hinge, but also exerts anisotropic tension on the adjacent wing-blade region, causing it to elongate and narrow. Reshaping of the wing blade occurs as constituent cells flow proximally with different velocities, generating reproducible patterns of flow, shear and rotation. These patterns result from a combination of oriented cell division, cell elongation and neighbor exchanges that are guided by the anisotropic stresses.

This scenario, where externally generated forces have an important role in epithelial remodeling differs from other convergent-extension events where autonomous cell movements actively drive tissue shape changes (Bertet et al., 2004; Blankenship et al., 2006; Keller et al., 2008; Rauzi et al., 2008; Zallen and Wieschaus, 2004). Externally induced epithelial stretching has been proposed to provoke stress-relieving rearrangements during *Drosophila* germband extension (Butler et al., 2009), and in the amphibian ectoderm (Keller et al., 1992, 2008). But in these cases movements of the underlying mesoderm, rather than contraction of adjacent epithelial cells, provides the external force. The *Drosophila* pupal wing will be a powerful system for uncovering molecular mechanisms underlying stress-induced epithelial remodelling.

The mechanisms specifying global PCP domain alignment have been elusive and controversial (Axelrod, 2009; Casal et al., 2006; Lawrence et al., 2007; Ma et al., 2003; Tree et al., 2002a). It had been thought that PCP proteins in the *Drosophila* wing are initially randomly distributed, but become intracellularly polarized along the PD axis starting approximately 10 hr before hair formation (Strutt and Strutt, 2005; Vladar et al., 2009; Wu and Mlodzik, 2009; Zallen, 2007). This led to the search for a global polarizing signal that operated at this time. Here, we show that PD orientation of PCP complexes does not arise from a random distribution; rather it evolves from a different global polarity pattern present at the prepupal-pupal transition. At this stage, PCP domains are organized such that Fz-containing domains face the wing margin rather than distally. Our previous work identified a similar global polarity pattern in prepupal wings, and showed that even larval wing discs show a global pattern of PCP (Classen et al., 2005). Thus PCP domains are always polarized, but their global orientation evolves dynamically during development.

What causes global reorientation of PCP during phase I, and the subsequent increase in the magnitude of polar order during phase II of wing-blade remodeling? During phase I, margin-oriented polarity is reoriented by specific patterns of local rotation and shear due to cell flows caused by hinge contraction. Local tissue rotation and shear reorient PCP domains by simple physical rules (see Equation [2] and Figure S7) similar to those that reorient molecular order in liquid crystal hydrodynamics. A significant fraction of PCP reorientation is produced by local tissue rotation alone. However, tissue shear also helps rotate polarity toward the shear axis. Simulations suggest that shear caused by oriented cell divisions, cell rearrangements and PD cell elongation can all contribute to polarity reorientation. One mechanism that may underlie the effect of cell elongation on PCP is the tendency of microtubules to align with the long axis of the cell. Indeed microtubules are aligned with the PD axis of wing epithelial cells and are essential for delivery of PCP proteins to the cortex (Shimada et al., 2006). Significantly, under conditions where normal PD polarity does not develop (e.g., in *ds* mutant wings or in severed wings), oriented cell division, cell rearrangements and cell elongation are disturbed. During phase II, oriented cell boundary rearrangements increase hexagonal packing geometry and improve PCP order. Simulations suggest this may occur via an annealing process that relaxes irregular cell packing to a more ordered hexagonal lattice with improved PCP order.

The atypical Cadherins Ft and Ds are needed to evolve the global PD polarity pattern. Exactly how they influence the global pattern has been controversial (Axelrod, 2009; Lawrence et al., 2007). It was proposed that this pathway provides a PD polarity cue that depends on higher relative levels of Ds expression in the hinge. This inhomogeneity was thought to generate intracellular asymmetry of Ft/Ds heterodimers throughout the wing, directly generating a small bias in Fz activity within each cell that could then be amplified to produce strong and stable alignment of PCP domains with the PD axis (Ma et al., 2003; Tree et al., 2002a). But the fact that uniform Ds expression suffices to rescue polarity in *ds* wings argues against this view (Matakatsu and Blair, 2004) (Figures S6G–S6I). Furthermore, Ft and Ds do not appear to act directly on core PCP proteins in the *Drosophila* abdomen (Casal et al., 2006). We propose that the Ft/Ds pathway influences the global PCP pattern, not by generating intracellular asymmetries that directly regulate PCP signaling, but indirectly through its effects on epithelial dynamics during both larval and pupal stages. Time-controlled loss of Ds shows that it is required throughout development for evolution of PD polarity (Figures S6D–S6F) (see also (Matakatsu and Blair, 2004)). During larval stages, Ds may guide the development of early margin-oriented polarity through its influence on oriented growth; our simulations suggest that oriented cell division strongly influences the global axis of planar polarity. Later, during hinge contraction and wing-blade remodeling, Ds is required for the oriented cell division and cell elongation that occur in response to anisotropic stresses. Both processes influence the polarity axis in vertex model simulations.

In future, it will be interesting to examine the roles of anisotropic growth and local morphogen signaling in establishing the global PCP pattern as wing discs grow. Our theoretical analysis shows that large scale planar polarity can be stably maintained during growth even in the absence of global polarizing signals. This is possible because polarity easily aligns over a few cell diameters without orientation defects, and subsequent cell rearrangements due to cell division do not destroy this order during growth. Thus, polarity that was initially established when the tissue was small can be expanded during growth, and any anterior-posterior or dorsal-ventral boundary-derived signal would not need to act directly over long distances.

The coupling of planar polarity to epithelial dynamics is a robust and flexible mechanism for coordinating tissue shape with planar polarity of constituent cells and may generalize to other systems. Indeed, mutations in the Wnt pathway perturb both convergent extension and the planar orientation of sensory hair cells in the mouse cochlea (Wang et al., 2005). Furthermore, the planar polarity of sensory hair cells in the lateral line organ of zebrafish is oriented by the direction of cell migration rather than long-range secreted cues (Lopez-Schier et al., 2004). Our theoretical analysis suggests that shear caused by stretch-induced rearrangements or by oriented cell divisions can reorient polarity either perpendicular or parallel to the shear axis, depending on the relative rates of shear and PCP turnover. Thus, this process is also highly versatile, and could be a fundamental principle of tissue organization.

EXPERIMENTAL PROCEDURES

Imaging

Pupae were prepared for imaging as described (Classen et al., 2008). Images were acquired with a Leica TCS-SP2 or an Olympus FV-1000 microscope. 20× and 40× oil immersion objectives were used to follow cell flows and global morphological changes occurring in the wing. A 63× oil immersion objective was used to image pupal wings with cellular resolution. Imaging was performed at 25° ± 2°C, or at 29°C using a Bachhoffer chamber.

Wing Wounding

Wings were wounded by gently scratching the pupal cuticule in the hinge region of the wing using forceps just before imaging (at around 15 hAPF).

Image Analysis and Figures

Z projections were created with ImageJ. For image analysis, we developed "packing analyzer v2.0", which measures cell areas, perimeter, packing, elongation, polarity, cell divisions and tracks the cells and their boundaries. Briefly, images are segmented using the watershed algorithm (Vincent and Soille, 1991). Each watershed catchment's basin is defined as a cell. Vertices are defined as pixels shared between three or more cells. Cell boundaries are identified as pixels shared by exactly two cells. Cell boundaries smaller than three pixels are reclassified as vertices. The polygon class is determined by counting cell vertices. Cell area is defined as the number of pixels in each cell. Cell perimeter is defined as the sum of the distance between all the pixels surrounding a cell. To track cells, we assign a unique identity to each in the first movie frame. Cells are then re-identified in the next images based on their positions and neighborhoods. Boundaries are defined by the two cells that share them. Division orientation is defined by a line connecting the centers of the two daughter cells, and the angle it makes with the PD axis (which is plotted as horizontal).

Movies created using our software were compressed using FFmpeg or Quicktime Pro. Graphs were created using Microsoft Excel, Gnuplot and Grace. Images were vectorized using Batik. Figures were composed with Adobe Illustrator.

SUPPLEMENTAL INFORMATION

Supplemental Information includes Extended Experimental Procedures, Supplemental Theoretical Procedures, seven figures, and seven movies and can be found with this article online at doi:10.1016/j.cell.2010.07.042.

ACKNOWLEDGMENTS

This work represents a truly collaborative effort. Each author has contributed significantly to the findings and regular group discussions guided the development of the ideas presented here. The manuscript was written jointly by all authors. S.E., A.S., J.R., R.F., and F.J. were supported by the Max Planck Gesellschaft. B.A. was funded by the Fondation pour la Recherche Médicale. D.S. acknowledges the Natural Sciences and Engineering Research Council of Canada and the German Academic Exchange Service. J.R. was supported by a predoctoral fellowship from the Boehringer Ingelheim Fonds. We thank Tony Hyman and Stephan Grill for use of the laser cutting microscope. We are grateful to Stephan Grill, Ewa Paluch, Elisabeth Knust, and Carl-Philipp Heisenberg for critical comments on the manuscript. We thank David Strutt, Seth S.Blair, VDRC and the Bloomington Stock Center for providing fly stocks, Barry Dickson for DNA constructs, Julia Gäbel for help with cloning, Sven Ssykor for transgenic injections.

Received: August 28, 2009
Revised: May 11, 2010
Accepted: July 23, 2010
Published: September 2, 2010

REFERENCES

Adler, P.N., Charlton, J., and Liu, J. (1998). Mutations in the cadherin superfamily member gene dachsous cause a tissue polarity phenotype by altering frizzled signaling. Development *125*, 959–968.

Amonlirdviman, K., Khare, N.A., Tree, D.N., Chen, W., Axelrod, J., and Tomlin, C.J. (2005). Mathematical modeling of planar cell polarity to understand domineering non-autonomy. Science *307*, 423–426.

Axelrod, J.D. (2009). Progress and challenges in understanding planar cell polarity signaling. Semin. Cell Dev. Biol. *20*, 964–971.

Baena-Lopez, L.A., Baonza, A., and Garcia-Bellido, A. (2005). The orientation of cell divisions determines the shape of Drosophila organs. Curr. Biol. *15*, 1640–1644.

Bertet, C., Sulak, L., and Lecuit, T. (2004). Myosin-dependent junction remodelling controls planar cell intercalation and axis elongation. Nature *429*, 667–671.

Blankenship, J.T., Backovic, S.T., Sanny, J.S., Weitz, O., and Zallen, J.A. (2006). Multicellular rosette formation links planar cell polarity to tissue morphogenesis. Dev. Cell *11*, 459–470.

Bryant, P.J., Huettner, B., Held, L.I., Jr., Ryerse, J., and Szidonya, J. (1988). Mutations at the fat locus interfere with cell proliferation control and epithelial morphogenesis in Drosophila. Dev. Biol. *129*, 541–554.

Burak, Y., and Shraiman, B.I. (2009). Order and stochastic dynamics in Drosophila planar cell polarity. PLoS Comput. Biol. *5*, e1000628.

Butler, L.C., Blanchard, G.B., Kabla, A.J., Lawrence, N.J., Welchman, D.P., Mahadevan, L., Adams, R.J., and Sanson, B. (2009). Cell shape changes indicate a role for extrinsic tensile forces in Drosophila germ-band extension. Nat. Cell Biol. *11*, 859–864.

Casal, J., Lawrence, P.A., and Struhl, G. (2006). Two separate molecular systems, Dachsous/Fat and Starry night/Frizzled, act independently to confer planar cell polarity. Development *133*, 4561–4572.

Chen, W.S., Antic, D., Matis, M., Logan, C.Y., Povelones, M., Anderson, G.A., Nusse, R., and Axelrod, J.D. (2008). Asymmetric homotypic interactions of the

atypical cadherin flamingo mediate intercellular polarity signaling. Cell *133*, 1093–1105.

Cho, E., and Irvine, K.D. (2004). Action of fat, four-jointed, dachsous and dachs in distal-to-proximal wing signaling. Development *131*, 4489–4500.

Clark, H.F., Brentrup, D., Schneitz, K., Bieber, A., Goodman, C., and Noll, M. (1995). Dachsous encodes a member of the cadherin superfamily that controls imaginal disc morphogenesis in Drosophila. Genes Dev. *9*, 1530–1542.

Classen, A., Anderson, K., Marois, E., and Eaton, S. (2005). Hexagonal Packing of Drosophila Wing Epithelial Cells by the Planar Cell Polarity Pathway. Dev. Cell *9*, 805–817.

Classen, A.K., Aigouy, B., Giangrande, A., and Eaton, S. (2008). Imaging Drosophila pupal wing morphogenesis. Methods Mol. Biol. *420*, 265–275.

Cortes, S., Glade, N., Chartier, I., and Tabony, J. (2006). Microtubule self-organisation by reaction-diffusion processes in miniature cell-sized containers and phospholipid vesicles. Biophys. Chem. *120*, 168–177.

Daga, R.R., and Nurse, P. (2008). Interphase microtubule bundles use global cell shape to guide spindle alignment in fission yeast. J. Cell Sci. *121*, 1973–1980.

de Gennes, P.G., and Prost, J. (1993). The Physics of Liquid Crystals, Second Edition (Gloucestershire, UK: Clarendon Press).

Farhadifar, R., Roper, J.C., Aigouy, B., Eaton, S., and Julicher, F. (2007). The Influence of Cell Mechanics, Cell-Cell Interactions, and Proliferation on Epithelial Packing. Curr. Biol. *17*, 2095–2104.

Garoia, F., Grifoni, D., Trotta, V., Guerra, D., Pezzoli, M.C., and Cavicchi, S. (2005). The tumor suppressor gene fat modulates the EGFR-mediated proliferation control in the imaginal tissues of Drosophila melanogaster. Mech. Dev. *122*, 175–187.

Garoia, F., Guerra, D., Pezzoli, M.C., Lopez-Varea, A., Cavicchi, S., and Garcia-Bellido, A. (2000). Cell behaviour of Drosophila fat cadherin mutations in wing development. Mech. Dev. *94*, 95–109.

Haase, S.B., and Lew, D.J. (2007). Microtubule organization: cell shape is destiny. Curr. Biol. *17*, R249–R251.

Ishikawa, H.O., Takeuchi, H., Haltiwanger, R.S., and Irvine, K.D. (2008). Four-jointed is a Golgi kinase that phosphorylates a subset of cadherin domains. Science *321*, 401–404.

Joanny, J.F., Julicher, F., Kruse, K., and Prost, J. (2007). Hydrodynamic theory for multi-component active polar gels. N. J. Phys. *9*, 422.

Keller, R., Shih, J., and Sater, A. (1992). The cellular basis of the convergence and extension of the Xenopus neural plate. Dev. Dyn. *193*, 199–217.

Keller, R., Shook, D., and Skoglund, P. (2008). The forces that shape embryos: physical aspects of convergent extension by cell intercalation. Phys. Biol. *5*, 15007.

Lawrence, P.A., Struhl, G., and Casal, J. (2007). Planar cell polarity: one or two pathways? Nat. Rev. Genet. *8*, 555–563.

Le Garrec, J.F., Lopez, P., and Kerszberg, M. (2006). Establishment and maintenance of planar epithelial cell polarity by asymmetric cadherin bridges: a computer model. Dev. Dyn. *235*, 235–246.

Lopez-Schier, H., Starr, C.J., Kappler, J.A., Kollmar, R., and Hudspeth, A.J. (2004). Directional cell migration establishes the axes of planar polarity in the posterior lateral-line organ of the zebrafish. Dev. Cell *7*, 401–412.

Ma, D., Amonlirdviman, K., Raffard, R.L., Abate, A., Tomlin, C.J., and Axelrod, J.D. (2008). Cell packing influences planar cell polarity signaling. Proc. Natl. Acad. Sci. USA *105*, 18800–18805.

Ma, D., Yang, C.H., McNeill, H., Simon, M.A., and Axelrod, J.D. (2003). Fidelity in planar cell polarity signalling. Nature *421*, 543–547.

Matakatsu, H., and Blair, S.S. (2004). Interactions between Fat and Dachsous and the regulation of planar cell polarity in the Drosophila wing. Development *131*, 3785–3794.

Rauzi, M., Verant, P., Lecuit, T., and Lenne, P.F. (2008). Nature and anisotropy of cortical forces orienting Drosophila tissue morphogenesis. Nat. Cell Biol. *10*, 1401–1410.

Seifert, J.R., and Mlodzik, M. (2007). Frizzled/PCP signalling: a conserved mechanism regulating cell polarity and directed motility. Nat. Rev. Genet. *8*, 126–138.

Shimada, Y., Yonemura, S., Ohkura, H., Strutt, D., and Uemura, T. (2006). Polarized transport of Frizzled along the planar microtubule arrays in Drosophila wing epithelium. Dev. Cell *10*, 209–222.

Simons, M., and Mlodzik, M. (2008). Planar cell polarity signaling: from fly development to human disease. Annu. Rev. Genet. *42*, 517–540.

Strauss, B., Adams, R.J., and Papalopulu, N. (2006). A default mechanism of spindle orientation based on cell shape is sufficient to generate cell fate diversity in polarised Xenopus blastomeres. Development *133*, 3883–3893.

Strutt, H., and Strutt, D. (2002). Nonautonomous planar polarity patterning in Drosophila: dishevelled-independent functions of frizzled. Dev. Cell *3*, 851–863.

Strutt, H., and Strutt, D. (2005). Long-range coordination of planar polarity in Drosophila. Bioessays *27*, 1218–1227.

Strutt, H., and Strutt, D. (2008). Differential stability of flamingo protein complexes underlies the establishment of planar polarity. Curr. Biol. *18*, 1555–1564.

Tree, D.R., Ma, D., and Axelrod, J.D. (2002a). A three-tiered mechanism for regulation of planar cell polarity. Semin. Cell Dev. Biol. *13*, 217–224.

Tree, D.R., Shulman, J.M., Rousset, R., Scott, M.P., Gubb, D., and Axelrod, J.D. (2002b). Prickle mediates feedback amplification to generate asymmetric planar cell polarity signaling. Cell *109*, 371–381.

Uemura, T., and Shimada, Y. (2003). Breaking cellular symmetry along planar axes in Drosophila and vertebrates. J. Biochem. *134*, 625–630.

Villano, J.L., and Katz, F.N. (1995). four-jointed is required for intermediate growth in the proximal-distal axis in Drosophila. Development *121*, 2767–2777.

Vincent, L., and Soille, P. (1991). Watersheds in digital spaces: an efficient algorithm based on immersion simulations. IEEE *13*, 583–598.

Vinson, C., and Adler, P.N. (1987). Directional non-cell autonomy and the transmission of polarity information by the *frizzled* gene of *Drosophila*. Nature *329*, 549–551.

Vladar, E.K., Antic, D., and Axelrod, J.D. (2009). Planar cell polarity signaling: The developing cell's compass. Cold Spring Harb. Perspect. Biol. *1*, a002964.

Wang, J., Mark, S., Zhang, X., Qian, D., Yoo, S.J., Radde-Gallwitz, K., Zhang, Y., Lin, X., Collazo, A., Wynshaw-Boris, A., et al. (2005). Regulation of polarized extension and planar cell polarity in the cochlea by the vertebrate PCP pathway. Nat. Genet. *37*, 980–985.

Wu, J., and Mlodzik, M. (2008). The frizzled extracellular domain is a ligand for Van Gogh/Stbm during nonautonomous planar cell polarity signaling. Dev. Cell *15*, 462–469.

Wu, J., and Mlodzik, M. (2009). A quest for the mechanism regulating global planar cell polarity of tissues. Trends Cell Biol. *19*, 295–305.

Zallen, J.A. (2007). Planar polarity and tissue morphogenesis. Cell *129*, 1051–1063.

Zallen, J.A., and Wieschaus, E. (2004). Patterned gene expression directs bipolar planar polarity in Drosophila. Dev. Cell *6*, 343–355.

Zeidler, M.P., Perrimon, N., and Strutt, D.I. (2000). Multiple roles for four-jointed in planar polarity and limb patterning. Dev. Biol. *228*, 181–196.